Progress In Electromagnetics Research Letters, Vol. 113, 35–42, 2023

Differential Wideband Antenna on Organic Substrate at 240 GHz with a Differential Wirebond Package

Joachim Hebeler* **and Thomas Zwick**

Abstract—This letter investigates a differential, planar, and wideband antenna on a commercial organic printed circuit board (PCB) substrate at 240 GHz with a novel packaging concept to integrate massive monolithically integrated circuits (MMICs). The antenna utilizes multiple series resonators to achieve a bandwidth of 75 GHz around 240 GHz. A novel differential bond wire package solution from chip to antenna feeds the differential antenna from an on-chip Marchand balun. The fabrication of the antenna and interconnect are analyzed, and potential improvements for future works are highlighted. Measurement proves the function of the designed package, which is competitive to the state of the art.

1. INTRODUCTION

Current trends in 5G, 6G, and radar sensors aim at systems operating at frequencies above 100 GHz with transmission windows in the atmosphere at 140 GHz and 240 GHz [1, 2]. Shrinking wavelength is a big challenge in exploiting the entire bandwidth available at these frequencies. Antenna feature sizes hit the limits of Printed Circuit Board (PCB) manufacturing. While classical thin-film processes can produce the necessary feature sizes, they need more integration and commercial viability. Another issue is the interface between active circuits and the antenna, causing many designers to employ on-chip antennas with external lenses to enhance the gain and efficiency to usable levels.

This letter investigates a planar antenna on a commercial PCB process with a 60 µm thick RF substrate. Due to manufacturing constraints and process specifics, a four-layer PCB stack-up with 17 µm copper foils is used. A solid ground plane is chosen to avoid warping and deformation of the substrate and metal structures during manufacturing, as shown in Fig. 1. The antenna and connection developed in this work will serve in conjunction with a 60 Gbit/s transmitter [3]. A usable bandwidth

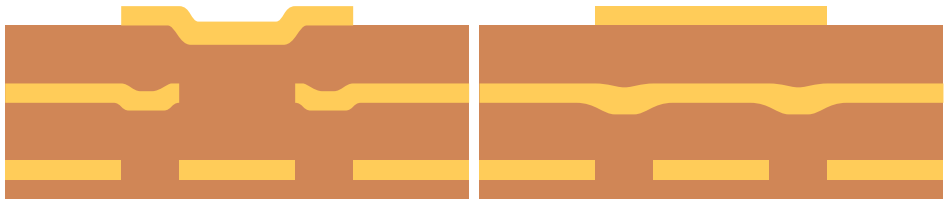

(a) With openings (b) With solid ground plane

Figure 1. Schematic cross-section view through the layers with the deformation visible due to openings in the lower metals layers (a) and the reduced effect over a solid ground plane (b).

Received 26 July 2023, Accepted 20 October 2023, Scheduled 31 October 2023

* Corresponding author: Joachim Hebeler (joachim.hebeler@kit.edu).
The authors are with the Institute of Radio Frequency Engineering and Electronics, Karlsruhe Institute of Technology, Karlsruhe, Germany.

of 50 GHz and a moderate gain of 6 dBi–10 dBi are targeted. The BPSK transmitter has a differential output; therefore, a differential antenna is investigated.

In [4], an antenna on an organic substrate was first demonstrated at 240 GHz whereas bond-wire interfaces at these frequencies were demonstrated in [5]. These publications focused on single-ended systems due to measurement constraints. In [6], differential bond wire interfaces and packaging concepts are presented, which are also employed for the antenna design presented here. In order to characterize the antenna separately from the interconnect, an on-chip balun and an on-substrate balun are used.

2. ANTENNA CONSTRUCTION

Antennas on PCBs are widely published and highly sophisticated. However, several factors hinder the full exploitation of proven wideband or efficient antenna structures in the application targeted here. The substrate thickness is limited by both availability and substrate wave suppression. Assuming an ϵ_r of 3.1 of the substrate, the wavelength at 240 GHz is 700 µm. The thickness should be less than 1/10th of the wavelength to avoid substrate waves. Therefore, a 60 µm substrate is chosen. This results in an aspect ratio of metal to substrate thickness of 1 : 3, which is rather low and implies large deformations in the case of openings in the ground plane or other layers underneath. The severe aspect ratio also influences the metal thickness, which can already vary from a minimum of 11.4 µm up to an unspecified maximum significantly over the nominal 17 µm thickness as per IPC-A-600J due to different material deposition or removal during processing. These factors lead to the decision for a solid ground plane on all lower layers to improve the flatness of the upper metal layers. Further, the minimum feature size of 40 µm is already 6% of the wavelength. This limits the application of more intricate designs, such as split-ring resonators or meta-materials.

Characterization of organic substrates at frequencies above 100 GHz is often lacking and suffers from the high variability of the heterogeneous structure of prepreg and core layers. The used material is *Megtron 6* from *Panasonic*, which, the manufacturer of the chosen prepreg, lists a range of 3.16 to 3.34 for the various core layers at 58 GHz and a range of 3.08 to 3.34 for the different prepreg layers. This variability is due to different epoxy-to-glass-fiber weave ratios. During the manufacturing of the PCB, this ratio and the final thickness of the layer change depending on the copper structure. This makes getting accurate design values without in situ measurements inherently tricky. The following design uses the datasheet value of 3.10.

The bandwidth of at least 50 GHz is achieved by using multiple series feed radiators on the continuous ground plane. This concept is a variation of series-fed differential patch antennas with nonuniform element size and spacing. Fig. 2(a) shows the manufactured geometry and dimensions of the top layer. Fig. 2(b) shows the realized antenna. Optimizing the parameterized model with an EM solver yields the final dimensions. The length of the antenna spans about $1.6\lambda_g$ in the substrate. The feed is designed to match 100 Ω differential impedance. The largest patch features an inset for matching. The last patch shorts the feed lines and has an inset for matching the wave impedance.

In order to evaluate the final thickness of the substrate layers and ϵ_r, a directly probable solution is desired. A rat-race balun enhanced by a second loop realizes the necessary single-ended to differential conversion. Fig. 2(c) shows the resulting layout and Fig. 2(d) the realized structure. The simulation indicates that the balun is slightly radiating itself. While undesired in most applications, it can be tolerated in this application as it only serves to validate the antenna.

A ground-signal-ground (GSG) probe pad is designed to contact the balun. It combines a via transition and capacitive coupling to the ground plane to enhance the bandwidth. To achieve the necessary probe pitch of 80 µm to 100 µm, the signal conductor is tapered down from 66 µm to 40 µm. The transition is optimized using EM simulations and a model for the probe.

The targeted packing solution uses wire bonds to connect a chip to the antenna. This interface suffers from an impedance mismatch. Using an encapsulation helps push the differential transition's impedance to the targeted 100 Ω. A study on the bond wire dimensions and encapsulant dependency is presented in [6]. The main limitation of this transition is the pad capacitance, as the encapsulant cannot compensate for it. On-chip, this capacitance is non avoidable. On the PCB, it is possible to taper down the differential lines to compensate for the fringing field at the end of the transmission line, thus enhancing the bandwidth. Two antenna setups are measured as follows:

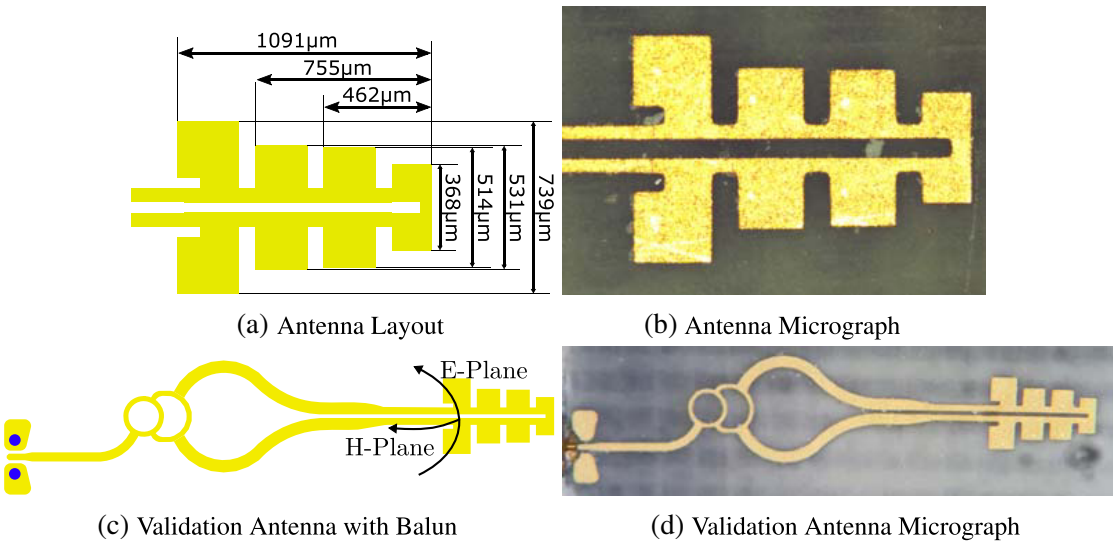

(a) Antenna Layout (b) Antenna Micrograph

(c) Validation Antenna with Balun (d) Validation Antenna Micrograph

Figure 2. The realized antenna geometries. Four resonators enhance the bandwidth of the antenna. The first antenna element has an inset to match the feed line. The fourth resonator shorts the feed line. The dimensions are shown in the layout view in (a) and the micrograph in (b). To validate the design, an on-substrate balun is designed. The layout is shown in (c), the micrograph in (d).

- *Validation antenna* with the on-substrate rat-race balun to probe the antenna on PCB directly
- *Packaged antenna* with on-chip balun and bond wire interconnect

3. PCB MANUFACTURING

The manufactured samples are first measured to evaluate the PCB manufacturing process. In order to evaluate the stack-up and glass-weave density, the PCBs are cut using a picosecond laser. Fig. 3(a) shows the cross-section along the probe pad, including the VIA connection. While the metal thickness is close to the nominal 17 µm with a final thickness of 18.8 µm, the prepreg layer thickness is reduced from the design value of 60 µm to 52 µm. Another issue visible is the inhomogeneous nature of the PCB substrate layers. The strands of the glass-fiber weave have a thickness of 30 µm to 40 µm, a significant amount of the thickness of the prepreg layer. The dents in the lower copper layer visible in Fig. 3(a) is an artifact from the laser cutting. Fig. 3(b) shows the cross-section through the antenna element. The

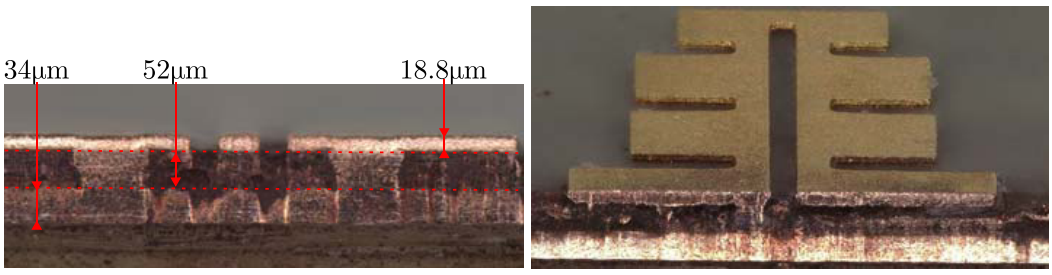

(a) The cross section of the Probe Feeding structure (b) Angled View at the cross section at an antenna

Figure 3. Cross section through the PCB for the probe pad (a) and antenna (b). Also, in (a) the VIA is visible. The top metal has a thickness of 18 µm, the lower metal has a thickness of 34 µm. The substrate has a thickness of 52 µm.

ground layer shows a very smooth surface, while the antenna metal has a more severe roughness, which is not visible in Fig. 3(a). This roughness may be nonuniform over the PCB. Also clearly visible are the random strands of glass fiber.

Next, all antenna dimensions were measured using a microscope to quantify the manufacturing tolerances. Narrow trenches, especially the channel between differential lines and the inset, have deviations up to 20 µm (33% of the nominal value). On average, all edges are 8 µm over etched with specific geometries suffering more. Further all inside 90° angles got rounded by 15 µm. As all antennas were built on the same PCB, no corrections to the design could be made.

4. VALIDATION ANTENNA RESULTS

The validation antenna is measured to ensure the PCB manufacturing yielded working antennas. Fig. 4(a) shows the measured and simulated return losses. All four measured samples deviate significantly from the simulation. While the simulation expects a resonance at 270 GHz, the measurement shows this resonance at approx. 285 GHz. This deviation does not result from mechanical deviations, as the simulation already includes this. Therefore, this has to result from a change in ϵ_r due to a different glass-weave-to-filler ratio. An effective ϵ_r of 2.9 matches simulation and measurement results as shown in purple in Fig. 4(a).

As the probe pad is relatively large, the influence of different probe placements is investigated to quantify the uncertainty of the pattern measurement. In order to illustrate the influence of the probe placement, one sample is measured multiple times with deviations from the nominal probe position, shown in Fig. 4(b). Depending on the contact, some significant variation is present, increasing the uncertainty of the measurements. Nevertheless, the frequency of critical resonances seems independent of the probe positioning. Above 280 GHz, some measurements show a significantly better input match than anticipated, hinting at probe-pad interactions causing radiation or losses. Fig. 4(a) shows the measurement of the four available samples. Samples three and four have over- and under-etching compensation applied to them, respectively. However, this geometry change is not visible in the measurements as it is impossible to distinguish whether the difference in the measured insertion loss is due to the etching compensation or the measurement uncertainty.

The measured radiation pattern for the validation antenna at 240 GHz in the E-plane is shown in Fig. 5. The measured and simulated radiation patterns agree well, except for the gain, which deviates by approximately 3 dB. This loss might be due to the increased copper surface roughness. More likely, it results from a slight tilt in the antenna as the radiating balun causes significant ripples in the H-plane.

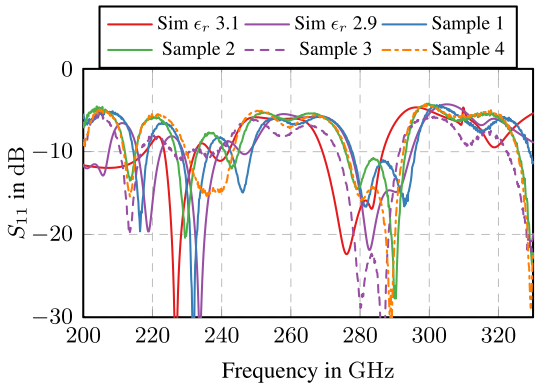

(a) Measured and simulated S_{11} of the validation antenna

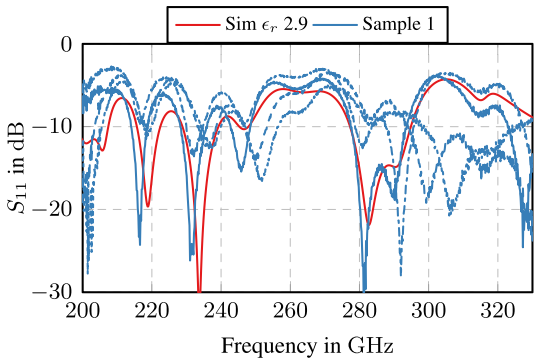

(b) Measurement repeatability over multiple contacts of the same sample

Figure 4. Simulated and measured return losses for the validation antenna. (a) shows the comparison between measurement and simulation for four measured samples. The simulation differs significantly due to a wrong ϵ_r. (b) shows the measurement repeatability over multiple contacts of the same sample. The transition from probe to PCB is very sensitive to probe placement.

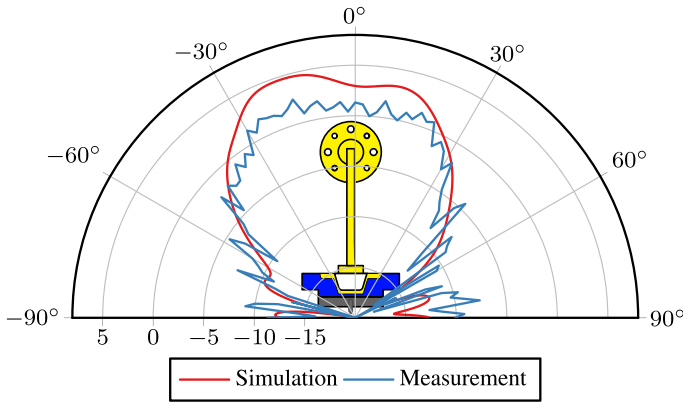

Figure 5. Measured and simulated patterns for the validation antenna at 240 GHz.

5. PACKAGED ANTENNA RESULTS

An on-chip marchand balun in a CMOS process transforms the single-ended probe into the necessary differential chip pads, providing a suitable interface for the antenna. The package is measured with and without encapsulation to compare the effect. The manufacturing process is shown in Figs. 6(a) and 6(b). The balun is placed and aligned to the PCB on a carrier. The connection is bonded with 17 µm gold bond wire and finally encapsulated.

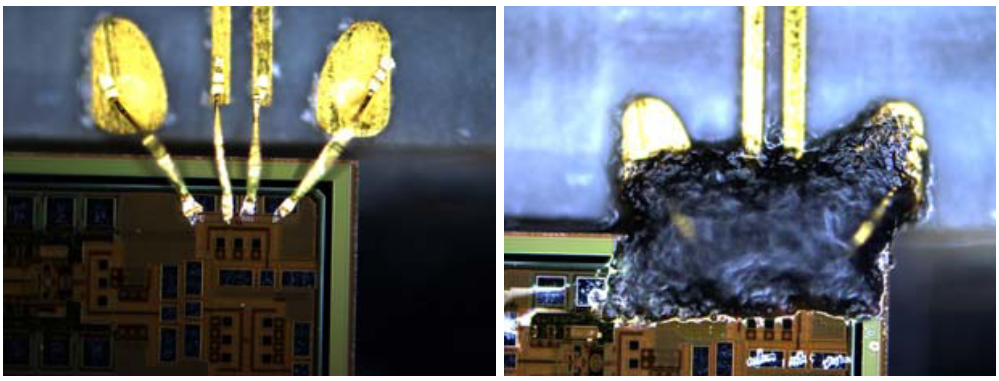

(a) Before encapsulation (b) After encapsulation

Figure 6. Micrograph of the differential interconnect package with the antenna and on-chip balun, before (a) and after encapsulation (b).

Figure 7(a) shows the measured and simulated S_{11} for one antenna sample before and after encapsulation. Overall, the simulation and measurement show decent agreement. Some resonances shift in frequency, and the simulated input match without encapsulation is worse than measured one as some effects above 245 GHz are not accurately captured. The measured input match −10 dB bandwidth for the final antenna is approximately 75 GHz from 205 GHz to 280 GHz, 10 GHz more than simulated.

Figures 8(a) and 8(b) show the measured radiation pattern. A clear improvement of at least 5 dB with the encapsulation is visible. The measured pattern agrees with the simulation, although the beam seems narrower. The measurements show many ripples not present in the simulation, indicating an interaction with the probe or measurement setup itself. There is an agreement between the measured validation antenna and the bonded antenna.

The simulated gain of the antenna element is plotted to compare the loss through the transition and feed. A drop about 3.7 dB in boresight is present, which matches roughly the estimated 2 dB loss in

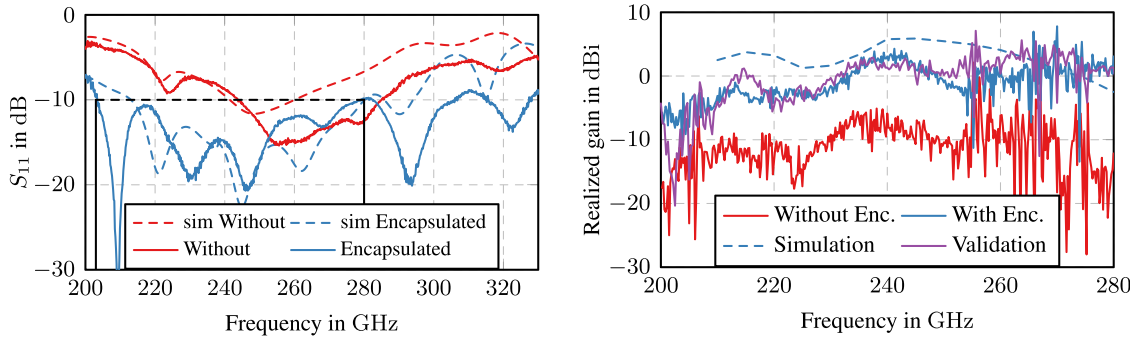

(a) Input match (b) Gain over Frequency

Figure 7. Measured and simulated input match (a) and gain at boresight (b) over frequency for the antenna without and with encapsulation. A clear improvement of the antenna performance with encapsulation and a match to the validation antenna is visible.

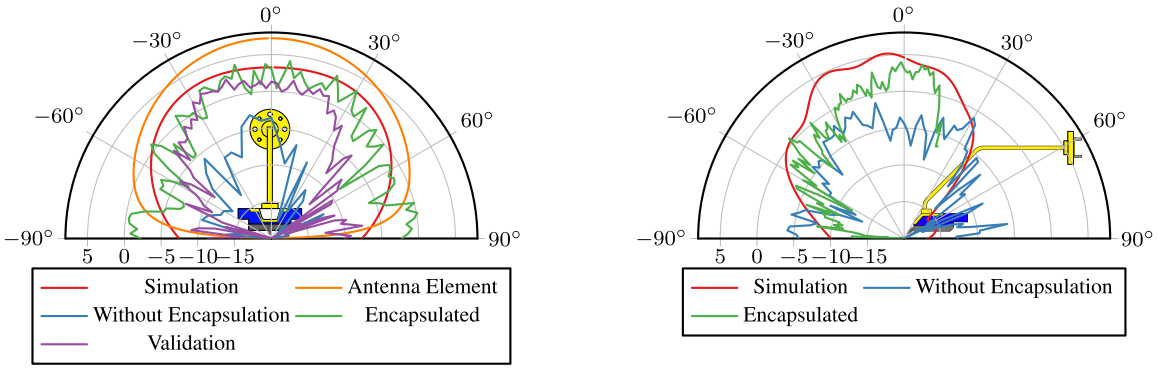

(a) *E* Plane (b) *H* Plane

Figure 8. Simulated and measured pattern of the realized antennas at 240 GHz with and without encapsulation. (a) shows the *E*-plane and (b) the *H*-plane.

the bond wire transition and 1.2 dB in the balun itself, as well as the additional loss in the longer feed. The simulation has a feed length of 0.5 mm to speed up the simulation, while the fabricated antenna has a feed length of 2 mm. Fig. 7(b) shows the gain over frequency at boresight for the validation antenna and the measured sample before and after encapsulation and the simulation. The strong ripple is an artifact of the used frequency extenders. Considering the losses of 3.7 dB, simulation and measurement agree until 250 GHz, where the measured samples seem to have higher losses.

Table 1. Comparison to the state of the art.

Ref.	Topology	Gain, dBi	f_c, GHz	BW, GHz
This.	Multiple Resonators	6*, 3.2	242.5	75, 31%
[4]	Slot-feed patch	7	235	32, 14%
[8]	Loop antenna	7*	305	90, 29.5%
[9]	On-chip patch with LBE	7	163	14, 4,3%
[7]	Slot bow-tie eWLB	4.2	250	100, 40%
[10]	Higher Order Mode Array	13.5	215	54.5, 25.4%
				*Simulation

A comparison to the state of the art of differential antennas is made in Table 1. The antenna presented here achieves 31% relative bandwidth, which is better than most other planar antennas in a comparable frequency range. Only the antenna presented in [7] achieves a higher relative bandwidth. However, it has a lower gain.

6. CONCLUSION

In this work, a differential antenna on a commercial PCB process is realized and operates from 205 GHz to 280 GHz. It features a differential feed bonded to a silicon IC, which, to the best of the authors' knowledge, is the first differential antenna on an organic substrate above 200 GHz and the first to be fed directly differentially from an IC. The antenna itself features an input 10 dB bandwidth of 75 GHz with a measured antenna gain about 3.2 dBi. Deducting the losses of the transition of about 3.5 dB, of which 1.2 dB are in the balun itself, an antenna gain about 6.7 dB is achieved, which is in line with the simulations. This result is competitive with state-of-the-art differential antennas.

Further improvements to the antenna geometry can be made to reduce the frequency scanning effect and to include manufacturing deviations. The results show the feasibility of fully integrating DC routing, baseband signaling, and the MMIC from [3] into a complete system.

ACKNOWLEDGMENT

This work was supported by the Deutsche Forschungsgemeinschaft (DFG) in the framework of the project ADAMIS (project number 394221495).

REFERENCES

1. Rajatheva, N., I. Atzeni, E. Bjornson, A. Bourdoux, S. Buzzi, J.-B. Dore, S. Erkucuk, M. Fuentes, K. Guan, Y. Hu, X. Huang, J. Hulkkonen, J. M. Jornet, M. Katz, R. Nilsson, E. Panayirci, K. Rabie, N. Rajapaksha, M. Salehi, H. Sarieddeen, T. Svensson, O. Tervo, A. Tolli, Q. Wu, and W. Xu, "White paper on broadband connectivity in 6G," 2020.
2. De Lima, C., D. Belot, R. Berkvens, A. Bourdoux, D. Dardari, M. Guillaud, M. Isomursu, E.-S. Lohan, Y. Miao, A. N. Barreto, M. R. K. Aziz, J. Saloranta, T. Sanguanpuak, H. Sarieddeen, G. Seco-Granados, J. Suutala, T. Svensson, M. Valkama, B. Van Liempd, and H. Wymeersch, "Convergent communication, sensing and localization in 6G systems: An overview of technologies, opportunities and challenges," *IEEE Access*, Vol. 9, 26902–26925, 2021.
3. Steinweg, L., J. Hebeler, T. Meister, T. Zwick, and F. Ellinger, "8.0-pj/bit bpsk transmitter with LO phase steering and 52-Gbps data rate operating at 246 GHz," *IEEE Transactions on Microwave Theory and Techniques*, 1–10, 2023.
4. Lacombe, E., F. Gianesello, A. Bisognin, C. Luxey, D. Titz, H. Gulan, and T. Zwick, "240 GHz antenna integrated on low-cost organic substrate packaging technology targeting high-data rate sub-THz telecommunication," *2017 47th European Microwave Conference (EuMC)*, 164–167, 2017.
5. Schafer, J., D. Müller, T. Zwick, G. Eren, and I. Kallfass, "Tx front end concept for FMCW radar with frequency scanning antenna at 240 GHz," *2018 International Workshop on Antenna Technology (iWAT)*, 1–4, 2018.
6. Hebeler, J., L. Steinweg, and T. Zwick, "Differential bondwire interface for chip-to-chip and chip-to-antenna interconnect above 200 GHz," *2022 52nd European Microwave Conference (EuMC)*, 306–309, 2022.
7. Ahmed, F., M. Furqan, and A. Stelzer, "120-GHz and 240-GHz broadband bow-tie antennas in EWLB package for high resolution radar applications," *2018 48th European Microwave Conference (EuMC)*, 1109–1112, 2018.
8. Shaulov, E., S. Jameson, and E. Socher, "A zero bias J-band antenna-coupled detector in 65-nm CMOS," *IEEE Transactions on Terahertz Science and Technology*, Vol. 11, No. 1, 62–69, 2021.

9. Ahmad, W., M. Kucharski, H. Ng, and D. Kissinger, "A compact efficient D-band micromachined on-chip differential patch antenna for radar applications," *2019 IEEE International Symposium on Antennas and Propagation and USNC-URSI Radio Science Meeting*, 2201–2202, 2019.
10. Wu, P., K. Liu, and Z. Yu, "220 GHz high-gain substrate integrated antennas with low fabrication cost based on higher order mode and pcb technology," *IEEE Transactions on Antennas and Propagation*, Vol. 71, No. 1, 18–28, 2023.